Research Paper
Computational Methods for Differential Equations
http://cmde.tabrizu.ac.ir
Vol. *, No. *, *, pp. 1-19
DOI:10.22034/cmde.2025.66681.3139

Numerical solutions of the fractional-order Jaulent-Miodek coupled system via Caputo derivative: A Petrov-Galerkin finite element approach for nonlinear wave phenomena

Waleed Adel[1,2,*], **Moutaz Ramadan**[3,4], **Ibrahim Hanafy**[4], **Hayah Samy**[4,5]

[1]Nanoelectronics Integrated Systems Center, Nile University, Giza, 12588, Egypt.

[2]Department of Mathematics and Engineering Physics, Faculty of Engineering, Mansoura University, Mansoura 35516, Egypt.

[3]Department of Mathematics, College of Sciences and Humanities, Prince Sattam bin Abdulaziz University, Alkharj, Saudi Arabia.

[4]Department of Mathematics and Computer Sciences, Faculty of Science, Port-Said University, Egypt.

[5]Higher Institute for Engineering and Technology, Manzala, Egypt.

Abstract

This study investigates the fractional-order Jaulent–Miodek system, which models nonlinear wave propagation in dispersive media with memory effects. A Petrov–Galerkin finite element method (PG-FEM) based on the Caputo fractional derivative is employed to capture long-range temporal correlations and nonlocal interactions. The proposed scheme achieves high accuracy and computational efficiency in resolving compacton solutions, soliton interactions, and nonlinear wave structures, overcoming limitations of traditional finite difference and spectral methods. Numerical simulations show that reducing the fractional order ($\alpha < 1$) enhances dispersion and delays attenuation, consistent with behaviors observed in viscoelastic media, porous fluid dynamics, nonlinear optics, and biomechanical processes. Moreover, the results confirm that fractional-order models provide a more faithful representation of power-law wave decay and anomalous transport phenomena compared with classical integer-order formulations. These findings underscore the importance of fractional calculus in advancing the mathematical modeling of nonlinear wave systems and point to promising directions for adaptive numerical schemes and future experimental validation.

Keywords. Time fractional Jaulent-Miodek system, Petrov-Galerkin finite element method, Quintic B-splines, Nonlinear wave processes, Caputo fractional derivative.

2010 Mathematics Subject Classification. 65L05, 34K06, 34K28.

1. Introduction

Mathematical modeling serves as a vital bridge between pure and applied sciences, offering a structured framework for understanding and interpreting complex real-world phenomena. By translating the internal logic of intricate systems into mathematical language, models enable researchers to simulate scenarios, explore solutions, and optimize outcomes. These models find applications across diverse fields, including biology [1], physics [20], economics [21], and engineering. They are also instrumental in studying disease dynamics [16] and financial market behaviors. As the demand for precision and computational efficiency grows, mathematical modeling continues to evolve, incorporating innovative computational techniques and interdisciplinary approaches to tackle increasingly complex problems [34].

Ordinary differential equations (ODEs) involve functions of a single variable and their derivatives, while partial differential equations (PDEs) encompass functions of multiple variables, enabling a more comprehensive analysis of systems influenced by several factors [14], [30], [28]. These equations are indispensable in various scientific disciplines, modeling phenomena such as population dynamics, heat distribution, celestial motion [4], and fluid flows [3], [22]. Among the most intriguing solutions to certain PDEs are solitons, which represent stable, wave-like structures that maintain their shape while propagating at constant speeds [27]. Found in fields like fluid dynamics, nonlinear optics,

Received: 08 April 2025; Accepted: 07 July 2026.
∗ Corresponding authors. Email: wauof@nu.edu.eg.

and theoretical physics, solitons exemplify the profound connection between nonlinear dynamics and wave behavior, [25]. Their stability and unique properties make them a compelling subject of study, with practical applications in signal processing and quantum field theories. Understanding solitons not only advances mathematical research but also highlights the importance of differential equations in unraveling and manipulating natural phenomena [6], [24].

Fractional-order differential equations (FODEs) extend classical differential equations by introducing derivatives and integrals of non-integer orders [29]. These equations provide a robust framework for modeling systems with memory effects, hereditary properties, and anomalous behaviors that cannot be adequately described by integer-order models. Fractional operators, such as the Riemann-Liouville, Caputo, and Grünwald-Letnikov derivatives, enable FODEs to capture long-range dependencies and power-law dynamics. FODEs are widely used in viscoelasticity [13], signal processing [9], control theory, and biology [18], offering insights into complex systems with fractional dynamics. Their nonlocal nature and dependence on historical data make them versatile yet computationally demanding, necessitating advanced analytical and numerical methods for their solution.

This concept is further extended to fractional-order partial differential equations (FPDEs), which incorporate fractional derivatives into systems involving multiple independent variables, such as space and time. By applying fractional derivatives in spatial or temporal dimensions, FPDEs enable the modeling of complex phenomena like anomalous diffusion, wave propagation in heterogeneous media, and processes governed by long-range interactions. These equations are widely used in physics, finance, fluid dynamics, and materials science, where traditional PDEs fall short in capturing real-world complexities. The nonlocality of fractional derivatives in FPDEs adds significant mathematical depth, requiring innovative approaches such as the homotopy analysis method, spectral techniques, or wavelet-based collocation methods for their solution [2]. Together, FODEs and FPDEs form a unified framework for advancing the understanding and simulation of complex systems with fractional dynamics. The ability of fractional-order models to replicate experimental observations while maintaining computational efficiency underscores their superiority in applications such as viscoelasticity, fluid dynamics, and biological systems.

The general form of a fractional differential equation can vary, but it typically includes terms representing fractional derivatives, often denoted as D^q, where q is a real number indicating the order of the derivative. For instance, a simple fractional differential equation can be expressed as:

$$D^q y(t) + a(t)y(t) = f(t), \tag{1.1}$$

where $y(t)$ is the unknown function, $a(t)$ is a given function, and $f(t)$ is a source term. Different definitions of fractional derivatives, such as the Caputo and Riemann-Liouville definitions, influence the properties of the solutions significantly.

Applications of fractional differential equations span areas such as control theory, signal processing, and anomalous diffusion, among others. The solutions to these equations often exhibit behaviors that better capture the complexities of real-world systems compared to integer-order models. Time fractional differential equations (TFDEs) have revolutionized applied mathematics by enabling the modeling of processes with memory and hereditary properties [11], [19]. These equations enhance integer-order models by incorporating fractional derivatives, allowing researchers to study real-world problems dominated by historical dependencies. Such systems are prevalent in physics, engineering, and finance, with applications in anomalous diffusion [23], viscoelasticity, and chaotic systems.

The Jaulent-Miodek (JM) system is a set of nonlinear partial differential equations (PDEs) that describe the propagation of nonlinear waves in dispersive media. When extended to fractional-order derivatives, the system captures memory effects and long-range interactions, making it a powerful tool for modeling complex physical phenomena. The time-fractional Jaulent-Miodek system is given by:

$$\frac{\partial^\alpha \nu}{\partial \tau^\alpha} + \frac{\partial^3 \nu}{\partial \psi^3} + \frac{3}{2}\varphi\frac{\partial^3 \varphi}{\partial \psi^3} + \frac{9}{2}\frac{\partial \varphi}{\partial \psi}\frac{\partial^2 \varphi}{\partial \psi^2} - 6\nu\frac{\partial \nu}{\partial \psi} - 6\nu\varphi\frac{\partial \varphi}{\partial \psi} - \frac{3}{2}\frac{\partial \nu}{\partial \psi}\varphi^2 = 0, \tag{1.2}$$

$$\frac{\partial^\alpha \varphi}{\partial \tau^\alpha} + \frac{\partial^3 \varphi}{\partial \psi^3} - 6\frac{\partial \nu}{\partial \psi}\varphi - 6\nu\frac{\partial \varphi}{\partial \psi} - \frac{15}{2}\frac{\partial \varphi}{\partial \psi}\varphi^2 = 0, \tag{1.3}$$

$$\nu(\psi, 0) = \frac{1}{8}\lambda^2\left(1 - 4\mathrm{sech}^2\left(\frac{\lambda\psi}{2}\right)\right),$$

$$\varphi(\psi,0)=\lambda \text{sech}\left(\frac{\lambda\psi}{2}\right). \tag{1.4}$$

and boundary conditions as follows

$$\begin{aligned} &\nu(-10,\tau)=\nu(10,\tau)=0, && \nu_\psi(-10,\tau)=\nu_\psi(10,\tau)=0,\\ &\varphi(-10,\tau)=\varphi(10,\tau)=0, && \varphi_\psi(-10,\tau)=\varphi_\psi(10,\tau)=0. \end{aligned} \tag{1.5}$$

The exact solution of Eq. (1.2) and Eq. (1.3) at $\alpha=1$,

$$\nu(\psi,\tau)=\frac{1}{8}\lambda^2\left(1-4sech^2\left(\frac{\lambda}{2}\left(\psi+\frac{1}{2}\lambda^2\tau\right)\right)\right), \tag{1.6}$$

$$\varphi(\psi,\tau)=\lambda sech\left(\frac{\lambda}{2}\left(\psi+\frac{1}{2}\lambda^2\tau\right)\right). \tag{1.7}$$

where $\nu(\psi,\tau)$ and $\varphi(\psi,\tau)$ are the unknown functions representing wave profiles and $-10\le\psi\le 10,\tau\ge 0$, $\frac{\partial^\alpha}{\partial\tau^\alpha}$ denotes the Caputo fractional derivative of order α $(0<\alpha<1)$, and ψ and τ represent the spatial and temporal variables, respectively. The fractional derivative introduces memory effects into the system, enabling it to model processes with hereditary properties and power-law dynamics. This makes the time-fractional JM system particularly suitable for describing phenomena such as anomalous diffusion, viscoelastic wave propagation, and nonlinear optical solitons.

The system exhibits several key mathematical features, including strong nonlinearity due to terms like $\nu\frac{\partial\nu}{\partial\psi}$ and $\varphi\frac{\partial\varphi}{\partial\psi}$, which describe interactions between wave components, and dispersion arising from the third-order spatial derivatives $\frac{\partial^3\nu}{\partial\psi^3}$ and $\frac{\partial^3\varphi}{\partial\psi^3}$. These features are essential for modeling soliton solutions and capturing complex wave behaviors. The Caputo fractional derivative further enhances the system's ability to model memory-dependent processes, providing a more accurate representation of real-world phenomena compared to integer-order models.

The time-fractional JM system has broad applications in various fields. In viscoelastic materials, it models wave propagation with memory effects and power-law attenuation. In fluid dynamics, it describes anomalous diffusion and transport phenomena in porous media, which are common in geophysics and petroleum engineering[17]. In nonlinear optics, the system captures the dynamics of optical solitons in nonlinear media, where fractional effects arise due to material properties and energy dissipation[5]. Additionally, the system can model wave-like phenomena in biological systems, such as signal propagation in neural networks or muscle contractions. These applications highlight the system's versatility and its importance in advancing both theoretical and applied research[32].

By incorporating fractional derivatives, the time-fractional JM system provides a more realistic representation of complex physical processes, paving the way for advancements in computational modeling and experimental validation[12]. Its ability to accurately describe memory effects, nonlinear interactions, and dispersion makes it a valuable tool for studying wave propagation in diverse scientific and engineering contexts[31].

The Jaulent-Miodek (JM) equation is a prominent nonlinear partial differential equation that models the propagation of nonlinear waves in dispersive media. It has found extensive applications in fields such as fluid dynamics, nonlinear optics, and plasma physics due to its ability to describe soliton interactions and complex wave structures. The time-fractional Jaulent-Miodek system extends this framework by incorporating fractional derivatives, which introduce memory effects and long-range interactions[15]. This makes the system particularly suitable for modeling phenomena such as anomalous diffusion, viscoelastic wave propagation, and energy dissipation in heterogeneous media[7]. Unlike integer-order models, the fractional-order JM system provides a more accurate representation of real-world processes by capturing power-law dynamics and hereditary properties inherent in many physical systems. We chose the time-fractional JM system for its versatility in describing complex wave behaviors and its relevance to advanced applications in physics, engineering, and biology. By studying this system, we aim to deepen the understanding of fractional-order dynamics and develop robust numerical methods for simulating nonlinear wave phenomena in memory-dependent media[10].

This study deals with constructing and investigating a numerical method for the solution of the time-fractional Jaulent-Miodek (JM) system based on the Petrov–Galerkin finite element (PG-FEM) technique with Caputo fractional derivative. The methodology presented not only provides good accuracy and stability but also other features that extend its applicability to a range of fractional order and nonlinear dispersive waves. In a coherent fashion, the work aims to strengthen the bridge that exists between the focused areas of marvels in the field of fractional calculus and its applications towards modeling complex systems. It is worth mentioning that the results presented here are intended to fill up the puzzles on fractional differential equations and at the same time provide an effective computational environment for the nonlinear fractional systems. The novelty of the presented work lies within the following points:

(1) The study investigates the time-fractional Jaulent-Miodek (JM) system, a nonlinear wave equation that models dispersion effects and memory-dependent behavior.
(2) The Caputo fractional derivative is employed to generalize the RH equation, enabling the characterization of time-dependent non-local features.
(3) The proposed solution utilizes the Petrov-Galerkin finite element method, with quintic B-splines as basis functions for enhanced accuracy.
(4) Quintic B-splines are specifically applied for spatial discretization, balancing computational efficiency and precision.
(5) A comprehensive Von-Neumann stability analysis is conducted, demonstrating that the numerical scheme is unconditionally stable.
(6) Extensive numerical experiments are performed, showcasing the method's ability to capture nonlinear wave processes and handle a wide range of fractional orders.

The paper is organized as follows: Section 2 provides a comprehensive description of the fractional definitions that will be used later. In section 3, the technique is applied to reduce the proposed model (1.3). Section 4 outlines the initial conditions of the solution. The stability analysis of the proposed algorithm is presented in section 5. Section 6 discusses the main results obtained using the collocation technique. Finally, section 7 concludes the paper with remarks and suggestions for future work. Next, we will discuss fractional calculus basic concepts.

2. Fractional calculus

In this section, we introduce the three most commonly used fractional derivatives: the Caputo, Riemann-Liouville, and Grünwald-Letnikov fractional derivatives. These definitions generalize the concept of differentiation to non-integer orders and are widely employed in various fields such as physics, engineering, and biology to model systems with memory effects, anomalous diffusion, and other complex phenomena. Each of these fractional derivatives has unique properties and advantages, making them suitable for specific applications.

The Caputo fractional derivative of order $\alpha > 0$ for a function $f(t)$ is defined as:

$$D^{\alpha} f(t) = \frac{1}{\Gamma(n-\alpha)} \int_0^t \frac{f^{(n)}(\tau)}{(t-\tau)^{\alpha+1-n}}\, d\tau, \tag{2.1}$$

where n is the smallest integer greater than or equal to α (i.e., $n-1 \leq \alpha < n$), $f^{(n)}(\tau)$ denotes the n-th derivative of $f(\tau)$, and $\Gamma(\cdot)$ is the gamma function. For $0 < \alpha < 1$, the Caputo derivative simplifies to:

$$D^{\alpha} f(t) = \frac{1}{\Gamma(1-\alpha)} \int_0^t \frac{f'(\tau)}{(t-\tau)^{\alpha}}\, d\tau. \tag{2.2}$$

The Caputo derivative is particularly advantageous for modeling physical systems with well-defined initial conditions, as it avoids the singularity issues associated with other fractional derivatives.

The Riemann-Liouville fractional derivative of order $\alpha > 0$ is defined as:

$$D^{\alpha} f(t) = \frac{1}{\Gamma(n-\alpha)} \frac{d^n}{dt^n} \int_0^t \frac{f(\tau)}{(t-\tau)^{\alpha+1-n}}\, d\tau, \tag{2.3}$$

where n is the smallest integer greater than or equal to α. For $0 < \alpha < 1$, this derivative reduces to:

$$D^{\alpha} f(t) = \frac{1}{\Gamma(1-\alpha)} \frac{d}{dt} \int_0^t \frac{f(\tau)}{(t-\tau)^{\alpha}} \, d\tau. \tag{2.4}$$

The Riemann-Liouville derivative is widely used in mathematical analysis due to its strong theoretical foundation, but it can be less intuitive for modeling physical systems due to its dependence on fractional initial conditions.

The Grünwald-Letnikov fractional derivative of order $\alpha > 0$ is defined as:

$$D^{\alpha} f(t) = \lim_{h \to 0} \frac{1}{h^{\alpha}} \sum_{k=0}^{\infty} (-1)^k \binom{\alpha}{k} f(t - kh), \tag{2.5}$$

where h is the step size and $\binom{\alpha}{k}$ is the generalized binomial coefficient. For practical numerical computations, this derivative is often approximated as:

$$D^{\alpha} f(t) \approx \frac{1}{h^{\alpha}} \sum_{k=0}^{N} (-1)^k \binom{\alpha}{k} f(t - kh), \tag{2.6}$$

where N is the number of terms in the summation. The Grünwald-Letnikov derivative is particularly useful for numerical simulations due to its straightforward discretization and ease of implementation.

Each of these fractional derivatives offers unique advantages and is suited to specific types of problems. The Caputo derivative is preferred for physical modeling with well-defined initial conditions, the Riemann-Liouville derivative is favored for theoretical analysis, and the Grünwald-Letnikov derivative is widely used in numerical computations. Together, they provide a comprehensive toolkit for modeling and analyzing complex systems with fractional dynamics. Next, we will illustrate the application of Petrov-Galerkin Finite Element Technique to Jaulent–Miodek Coupled System.

3. Implementation Petrov-Galerkin finite element technique to Jaulent–Miodek coupled system

In this section, we will illustrate the main steps for solving model (1.3) using the Petrov-Galerkin finite element method. We first define model (1.3) throughout $[a, b]$ that is a finite region with boundary conditions. Next, let a partition of $[a, b]$ be $a = \psi_0 < \psi_1 < \ldots < \psi_N = b$ by the equally spaced knots ψ_i and let quintic B-splines with knots at the points ψ_i, $0 < i < N$ are $\phi_i(\psi)$ where the set $\phi_{i-2}, \phi_{i-1}, \phi_i, \phi_{i+1}, \phi_{i+2}, \phi_{i+3}$ constitutes a series of splines, serving as the basis for functions sought within the finite region $[a, b]$. The solution approximation $\nu_N(\psi, \tau)$ for $\nu(\psi, \tau)$ is defined as follows:

$$\nu_N(\psi, \tau) = \sum_{i=-2}^{N+2} \phi_i(\psi) \nu_i(\tau), \tag{3.1}$$

where ν_i represent time-dependent parameters that can be computed from boundary conditions.

$$\nu(a, \tau) = \nu(b, \tau) = 0, \qquad \nu_{\psi}(a, \tau) = \nu_{\psi}(b, \tau) = 0. \tag{3.2}$$

The solution approximation $\varphi_N(\psi, \tau)$ for $\varphi(\psi, \tau)$ is defined as follows:

$$\varphi_N(\psi, \tau) = \sum_{i=-2}^{N+2} \phi_i(\psi) \eta_i(\tau), \tag{3.3}$$

where φ_i represent time-dependent parameters that can be computed from boundary conditions.

$$\varphi(a, \tau) = \varphi(b, \tau) = 0, \qquad \varphi_{\psi}(a, \tau) = \varphi_{\psi}(b, \tau) = 0. \tag{3.4}$$

The intervals $[\psi_i, \psi_{i+1}]$ are utilized to define finite elements with nodes positioned at ψ_i and ψ_{i+1}. Each element $[\psi_i, \psi_{i+1}]$ is thus spanned by six splines $(\phi_{i-2}, \phi_{i-1}, \phi_i, \phi_{i+1}, \phi_{i+2}, \phi_{i+3})$, which are expressed within a local coordinate system denoted by ζ, defined as $h\zeta = (\psi - \psi_i)$ where $h = \psi_{i+1} - \psi_i$ and $0 \leq \zeta \leq 1$. The approximate solution in the quintic B-spline collocation method can be expressed as a combination of quintic B-spline basis functions for the

approximation of the space variables under consideration[26]. The formulations for all these splines across the element $[\psi_i, \psi_{i+1}]$ are given by:

$$\begin{aligned}
\phi_{i-2} &= 1 - 5\zeta + 10\zeta^2 - 10\zeta^3 + 5\zeta^4 - \zeta^5,\\
\phi_{i-1} &= 26 - 50\zeta + 20\zeta^2 + 20\zeta^3 - 20\zeta^4 + 5\zeta^5,\\
\phi_{i} &= 66 - 60\zeta^2 + 30\zeta^4 - 10\zeta^5,\\
\phi_{i+1} &= 26 + 50\zeta + 20\zeta^2 - 20\zeta^3 - 20\zeta^4 + 10\zeta^5,\\
\phi_{i+2} &= 1 + 5\zeta + 10\zeta^2 + 10\zeta^3 + 5\zeta^4 - 5\zeta^5,\\
\phi_{i+3} &= \zeta^5.
\end{aligned} \tag{3.5}$$

Outside the interval $[\psi_{i-3}, \psi_{i+3}]$, the spline $\phi_i(\psi)$ and its fifth derivatives are zero. When we utilize Eq. (3.3) to formulate equations based on the element parameters u_i^e, these curves serve as "shape" functions for the element.

The dashes denote differentiation with respect to ψ. Applying the Petrov–Galerkin method with the chosen weight functions $W = \phi(\psi)$ to Eq. (1.3) leads to the following weak formulations of the JM system:

$$\int_b^a W\left(\frac{\partial^\alpha \nu}{\partial \tau^\alpha} + \frac{\partial^3 \nu}{\partial \psi^3} + \frac{3}{2}\varphi\frac{\partial^3 \varphi}{\partial \psi^3} + \frac{9}{2}\frac{\partial \varphi}{\partial \psi}\frac{\partial^2 \varphi}{\partial \psi^2} - 6\nu\frac{\partial \nu}{\partial \psi} - 6\nu\varphi\frac{\partial \varphi}{\partial \psi} - \frac{3}{2}\frac{\partial \nu}{\partial \psi}\varphi^2\right) d\psi = 0. \tag{3.6}$$

$$\int_b^a W\left(\frac{\partial^\alpha \varphi}{\partial \tau^\alpha} + \frac{\partial^3 \varphi}{\partial \psi^3} - 6\frac{\partial \nu}{\partial \psi}\varphi - 6\nu\frac{\partial \varphi}{\partial \psi} - \frac{15}{2}\frac{\partial \varphi}{\partial \psi}\varphi^2\right) d\psi = 0. \tag{3.7}$$

Now, let's establish the corresponding element matrices. For the contribution of the standard element $[\psi_i, \psi_{i+1}]$, we acquire:

$$\int_e W\left(\nu^e_{\tau^\alpha} + \nu^e_{\psi^3} + \tfrac{3}{2}\varphi^e\varphi^e_{\psi^3} + \tfrac{9}{2}\varphi^e_\psi\varphi^e_{\psi^2} - 6\nu^e\nu^e_\psi - 6\nu^e\varphi^e\varphi^e_\psi - \tfrac{3}{2}\nu^e_\psi\varphi^{2e}\right) d\psi = 0, \tag{3.8}$$

$$\int_e W\left(\varphi^e_{\tau^\alpha} + \varphi^e_{\psi^3} - 6\nu^e_\psi\varphi^e - 6\nu^e\varphi^e_\psi - \tfrac{15}{2}\varphi^e_\psi\varphi^{2e}\right) d\psi = 0, \tag{3.9}$$

The $\nu_N(\psi, \tau)$ and $\varphi_N(\psi, \tau)$ variation across the element $[\psi_{i-3}, \psi_{i+3}]$ is provided by

$$\nu^e(\psi, \tau) = \sum_{j=i-2}^{i+3} \phi_j(\psi)\delta_i(\tau), \qquad \varphi^e(\psi, \tau) = \sum_{j=i-2}^{i+3} \phi_j(\psi)\delta_i(\tau). \tag{3.10}$$

$$\begin{aligned}
&\sum_{i=l-2}^{l+3}\left(\int_{\psi_l}^{\psi_{l+1}} \phi_k\phi_i\, d\psi\right) D^\alpha_\tau \nu_j(\tau)^e_i + \sum_{i=l-2}^{l+3}\left(\int_{\psi_l}^{\psi_{l+1}} \phi_k\phi_i'''\, d\psi\right)\nu^e_i\\
&- 6\sum_{j=l-2}^{l+3}\sum_{i=l-2}^{l+3}\left(\left(\int_{\psi_l}^{\psi_{l+1}} \phi_k\phi_i\phi_j'\, d\psi\right)\nu^e_i\right)\nu^e_j - 6\sum_{j=l-2}^{l+3}\sum_{i=l-2}^{l+3}\left(\left(\int_{\psi_l}^{\psi_{l+1}} \phi_i\phi_i\phi_j\phi_k'\, d\psi\right)\nu^e_i\varphi^e_i\right)\varphi^e_j\\
&- \frac{3}{2}\sum_{j=l-2}^{l+3}\sum_{i=l-2}^{l+3}\left(\left(\int_{\psi_l}^{\psi_{l+1}} \phi_k\phi_i'\phi_j^2\, d\psi\right)\nu^e_i\right)\varphi^{2e}_i + \frac{3}{2}\sum_{j=l-2}^{l+3}\sum_{i=l-2}^{l+3}\left(\left(\int_{\psi_l}^{\psi_{l+1}} \phi_k\phi_i\phi_j'''\, d\psi\right)\varphi^e_i\right)\varphi^e_i\\
&+ \frac{9}{2}\sum_{j=l-2}^{l+3}\sum_{i=l-2}^{l+3}\left(\left(\int_{\psi_l}^{\psi_{l+1}} \phi_k\phi_i'\phi_j''\, d\psi\right)\varphi^e_i\right)\varphi^e_j = 0,
\end{aligned} \tag{3.11}$$

$$\sum_{i=l-2}^{l+3}\left(\int_{\psi_l}^{\psi_{l+1}}\phi_k\phi_i\,d\psi\right)D_\tau^\alpha\varphi_j(\tau)_i^e+\sum_{i=l-2}^{l+3}\left(\int_{\psi_l}^{\psi_{l+1}}\phi_k\phi_i^{'''}\,d\psi\right)\varphi_i^e$$
$$-6\sum_{j=l-2}^{l+3}\sum_{i=l-2}^{l+3}\left(\left(\int_{\psi_l}^{\psi_{l+1}}\phi_k\phi_i^{'}\phi_j\,d\psi\right)\nu_i^e\right)\varphi_j^e-6\sum_{j=l-2}^{l+3}\sum_{i=l-2}^{l+3}\left(\left(\int_{\psi_l}^{\psi_{l+1}}\phi_i\phi_j\phi_k^{'}\,d\psi\right)\nu_i^e\right)\varphi_j^e$$
$$-\frac{15}{2}\sum_{j=l-2}^{l+3}\sum_{i=l-2}^{l+3}\left(\left(\int_{\psi_l}^{\psi_{l+1}}\phi_k\phi_i^{'}\phi_j^2\,d\psi\right)\varphi_i^e\right)\varphi_i^{2e}=0, \tag{3.12}$$

where $D_\tau^\alpha\nu_j(\tau)$ is defined by

$$D_\tau^\alpha f(t)=\frac{1}{\Gamma(1-\alpha)}\int_0^t\frac{f'(\tau)}{(t-\tau)^\alpha}\,d\tau \tag{3.13}$$

The matrix form is constructed as:

$$A^e\nu^{e\alpha}+B^e\nu^{eT}-6C^e\nu^{eT}\nu^{eT}-6D^2\nu^{eT}\varphi^{eT}\varphi^{eT}-\tfrac{3}{2}\nu^{eT}\varphi^{e2T}+\tfrac{3}{2}\varphi^{eT}\varphi^{eT}+\tfrac{9}{2}\varphi^{eT}\varphi^{eT}=0, \tag{3.14}$$

$$A^e\varphi^{e\alpha}+B^e\nu^{eT}-6H^e\nu^{eT}\varphi^{eT}-6C^2\nu^{eT}\varphi^{eT}\varphi^{eT}-\tfrac{15}{2}\varphi^{eT}\varphi^{e2T}=0, \tag{3.15}$$

$$\nu^e=(\nu_{l-2},\nu_{l-1},\nu_l,\nu_{l+1},\nu_{l+2},\nu_{l+3})^T,$$
$$\varphi^e=(\varphi_{l-2},\varphi_{l-1},\varphi_l,\varphi_{l+1},\varphi_{l+2},\varphi_{l+3})^T. \tag{3.16}$$

The element matrices are given by

$$A_{ij}^e=\int_{\psi_l}^{\psi_{l+1}}\phi_k\phi_i d\psi,\quad B_{ij}^e=\int_{\psi_l}^{\psi_{l+1}}\phi_k\phi_i^{'''}\,d\psi,\quad C_{ij}^e=\int_{\psi_l}^{\psi_{l+1}}\phi_i\phi_j\phi_k^{'}d\psi,\quad D_{ij}^e=\int_{\psi_l}^{\psi_{l+1}}\phi_k^2\phi_i\phi_j^{'}d\psi,$$
$$E_{ij}^e=\int_{\psi_l}^{\psi_{l+1}}\phi_k\phi_i^{'}\phi_j^2d\psi,\quad F_{ij}^e=\int_{\psi_l}^{\psi_{l+1}}\phi_k\phi_i\phi_j^{'''}\,d\psi,\quad G_{ij}^e=\int_{\psi_l}^{\psi_{l+1}}\phi_k\phi_i^{'}\phi_j^{''}d\psi,\quad H_{ij}^e=\int_{\psi_l}^{\psi_{l+1}}\phi_k\phi_i^{'}\phi_j d\psi \tag{3.17}$$

where i, j, and k range from $l-2$ to $l+3$ for the element $[\psi_l,\psi_{l+1}]$. Consequently, the matrices A^e and B^e are of size 6×6, while C^e, D^e,E^e,F^e,G^e and H^e are of size $6\times6\times6$. In our algorithm, instead of C^e, D^e,E^e,F^e,G^e and H^e, we employ the corresponding 6×6 matrices b^e, c^e, d^e, e^e, f^e, g^e and h^e.

$$B_{ij}^e=\sum_{k=l-2}^{l+3}b_{ijk}^e\nu_k^e,\quad C_{ij}^e=\sum_{k=l-2}^{l+3}c_{ijk}^e\nu_k^e,\quad D_{ij}^e=\sum_{k=l-2}^{l+3}d_{ijk}^e\nu_k^e,\quad E_{ij}^e=\sum_{k=l-2}^{l+3}e_{ijk}^e\nu_k^e,$$
$$F_{ij}^e=\sum_{k=l-2}^{l+3}f_{ijk}^e\nu_k^e,\quad G_{ij}^e=\sum_{k=l-2}^{l+3}g_{ijk}^e\nu_k^e,\quad H_{ij}^e=\sum_{k=l-2}^{l+3}h_{ijk}^e\varphi_k^e. \tag{3.18}$$

This is contingent on the variables ν_k^e. The matrix of elements A^e is algebraically determined from Eq. (3.17), where ν_k^e is provided by Eq. (3.16). The equation below is derived by assembling the elements from Eq. (3.14).

$$A\nu_{\tau^\alpha}+B\nu-6C\nu\nu-6D\nu\varphi\varphi-\tfrac{3}{2}E\nu\varphi^2+\tfrac{3}{2}F\varphi\varphi+\tfrac{9}{2}G\varphi\varphi=0, \tag{3.19}$$

$$A\varphi_{\tau^\alpha} + B\varphi - 6H\nu\varphi - 6C\nu\varphi - \tfrac{15}{2}E\varphi\varphi = 0, \tag{3.20}$$

where the matrices A, B, C, D, are constructed from the element matrices A^e, B^e, C^e, D^e respectively in the usual way and

$$\nu = (\nu_{-2}, \nu_{-1}, \nu_0, \cdots, \nu_{N+1}, \nu_{N+2})^T. \tag{3.21}$$

$$\varphi = (\varphi_{-2}, \varphi_{-1}, \varphi_0, \cdots, \varphi_{N+1}, \varphi_{N+2})^T. \tag{3.22}$$

We now assume that $\nu_j^n = 0$ and $\varphi_j^n = 0$ for $j = -2, -1, 0, N+1, N+2$, and $N+3$ in order to solve the system above. Thomas's method can be used to solve the nonlinear system in Eq. (3.14) and determine the unknown approximate solutions ν_j^n and φ_j^n. Thus, it is also possible to get the necessary solution to the Fractional-Order Jaulent–Miodek Coupled System.

4. The initial state

In this section, the initial state for solving system 3.19 is outlined. We initiate the time assessment of u^{n+1} by computing the vector u^0 from the initial condition using the recurrence relation (3.19). Referring to Eq. (3.5), if we rewrite the global trial functions as follows:

$$\nu_N(\psi, 0) = \sum_{i=-2}^{N+2} \phi_i(\psi)\nu_i^0, \qquad \varphi_N(\psi, 0) = \sum_{i=-2}^{N+2} \phi_i(\psi)\varphi_i^0. \tag{4.1}$$

The parameters ν_i^0 represent unknowns that need to be determined. To establish the initial vector ν_i^0, ν_N must satisfy the following conditions:

At the knots ψ_j, it agrees with the analytical initial condition; applying Eq. (3.5), it leads to $N+1$ conditions.

The solution of matrix equations is then used to get the start up vector ν^0 [26] ,

$$M\nu^0 = b, \tag{4.2}$$

where

$$M = \begin{bmatrix}
3 & 30 & 27 & & & & & & \\
1 & 18 & 33 & 8 & & & & & \\
1 & 26 & 66 & 26 & 1 & & & & \\
 & 1 & 26 & 66 & 26 & 1 & & & \\
 & & & \cdot & & & & & \\
 & & . & . & . & . & . & & \\
 & & & & & \cdot & & & \\
 & & & 1 & 26 & 66 & 26 & 1 & \\
 & & & & 1 & 26 & 66 & 26 & 1 \\
 & & & & & 8 & 33 & 18 & 1 \\
 & & & & & & 27 & 30 & 3
\end{bmatrix}, \tag{4.3}$$

$$b = (\nu^{''}(\psi_0), \nu^{'}(\psi_0), \nu(\psi_0), \nu(\psi_1), \cdots, \nu(\psi_N), \nu^{'}(\psi_N), \nu^{''}(\psi_N))^T,$$

$$\nu^0 = (\nu_{-2}^0, \nu_{-1}^0, \nu_0^0, \cdots, \nu_N^0, \nu_{N+1}^0, \nu_{N+2}^0)^T. \tag{4.4}$$

After determining the initial vector η^0 as the solution of the undecadiagonal matrix Eq. (3.14), the system is solved using a Thomas algorithm [33]. We conclude the following remark.

Remark 4.1. The Thomas algorithm was chosen for solving the system due to its computational efficiency and numerical stability, particularly when dealing with tridiagonal matrices arising from discretized fractional differential equations. Unlike general matrix solvers, the Thomas algorithm operates with $O(n)$ complexity, significantly reducing computational cost while ensuring fast and accurate solutions. Its direct approach eliminates the need for iterative refinement, making it well-suited for fractional-order systems, where precision in handling non-local effects is critical

Finally, the algorithm for evaluating the solution can be as follows

Algorithm 1 PG-FEM for Jaulent–Miodek coupled system.

procedure PG-FEM($N, M, \Delta\tau, \alpha$)
Define $\psi \in [a, b]$, $\tau \in [0, T]$; set N (space DOFs), M (time steps), $0 < \alpha \leq 1$
Build quintic B-spline basis $\{\phi_i(\psi)\}_{i=1}^{N}$
Spatial assembly: Assemble mass A and linear operator $\mathcal{K} = \mathcal{K}_s + \mathcal{K}_a$
Initial data: Project $\nu(\psi, 0)$, $\varphi(\psi, 0)$ onto the basis to form $\mathbf{C}^0 = [\boldsymbol{\nu}^0; \boldsymbol{\varphi}^0]$
Time weights (implicit L1/GL): Define $g_0 = 1$,
$g_k = (k+1)^{1-\alpha} - 2k^{1-\alpha} + (k-1)^{1-\alpha} \quad (k \geq 1)$
for $n := 0$ to $M - 1$ **do**
$\mathbf{H}^{n+1} \leftarrow \sum_{k=1}^{n} g_k \, \mathbf{C}^{n+1-k}$ (if $n = 0$, set $\mathbf{H}^1 = \mathbf{0}$)
Implicit step: Find $\mathbf{C}^{n+1}$ such that
$\frac{1}{\Delta\tau^{\alpha}} A\big(g_0 \, \mathbf{C}^{n+1} + \mathbf{H}^{n+1}\big) + \mathcal{K} \, \mathbf{C}^{n+1} = \mathcal{N}(\mathbf{C}^{n+1}) + \mathbf{f}^{n+1}$
end for
return $\{\mathbf{C}^n\}_{n=0}^{M}$ with $\mathbf{C}^n = [\boldsymbol{\nu}^n; \boldsymbol{\varphi}^n]$
end procedure

5. Stability analysis

In this section, we analyze the PG–FEM scheme obtained in section 3 for the time–fractional JM system with Caputo derivative. Let $\Delta\tau$ be the time step and $\{g_k\}_{k\geq 0}$ be the positive L1/Grünwald–Letnikov (GL) weights used in Algorithm 1. Denote by A the symmetric positive definite mass matrix and by $\mathcal{K}$ the assembled linear spatial operator. We split $\mathcal{K} = \mathcal{K}_s + \mathcal{K}_a$ with $\mathcal{K}_s^{\top} = \mathcal{K}_s \succeq 0$ and $\mathcal{K}_a^{\top} = -\mathcal{K}_a$, a standard property for the present Petrov-Galerkin discretization under periodic or clamped boundary conditions. The nonlinear terms are collected into $\mathcal{N}(\cdot)$. Now, using the implicit L1/GL approximation of the Caputo derivative, the fully discrete system reads

$$A \, \frac{1}{\Delta\tau^{\alpha}} \sum_{k=0}^{n+1} g_k \, U^{n+1-k} \; + \; \mathcal{K} \, U^{n+1} \; = \; \mathcal{N}(U^{n+1}), \qquad U = [\nu; \, \phi], \tag{5.1}$$

which is the vector form corresponding to Eqs. (3.19)–(3.22) after assembly and stacking the coefficients. Now we will consider the Von-Neumann analysis for the linearized form of the system.

5.1. **Von-Neumann analysis (linearized system).** We first consider the linearized system $\mathcal{N} \equiv 0$ and assume a Fourier mode $U_j^n = z^n \mathrm{e}^{\mathrm{i}j\theta}$, $\theta \in [-\pi, \pi]$. Let $\widehat{A} > 0$ be the scalar symbol of A and let $\Lambda(\theta) = \mu(\theta) + \mathrm{i}\gamma(\theta)$ be the symbol of $\mathcal{K}$ on the mode, with $\mu(\theta) \geq 0$ and $\gamma(\theta) \in \mathbb{R}$. Taking symbols in (5.1) yields

$$\frac{\widehat{A}}{\Delta\tau^{\alpha}} \, \delta(z) \; + \; \Lambda(\theta) \; = \; 0, \qquad \delta(z) \; := \; \sum_{k=0}^{\infty} g_k \, z^{-k}. \tag{5.2}$$

For the L1/GL weights $g_k > 0$, the generating function $\delta(z)$ maps the unit disk $\{|z| < 1\}$ into a sector of the right half–plane and, in particular, satisfies $\Re\{\delta(z)\} > 0$ whenever $|z| < 1$. Since $\mu(\theta) \geq 0$, the term $-(\Delta\tau^{\alpha}/\widehat{A})\,\Lambda(\theta)$ lies in the closed left half–plane. Equation (5.2) therefore admits a root with $|z(\theta)| \leq 1$ for every θ and every $\Delta\tau > 0$, and if $\mu(\theta) > 0$ for any $\theta \neq 0$ then $|z(\theta)| < 1$ strictly. Hence the linearized scheme is *unconditionally stable*.
Seocnly, we will provide the proof of the discrete energy estimate for the nonlinear system.

5.2. **Discrete energy estimate (nonlinear system).** We now treat (5.1) with $\mathcal{N} \neq 0$. Taking the A–inner product with U^{n+1} and using $\langle \mathcal{K}_a U^{n+1}, U^{n+1} \rangle = 0$ and $\langle \mathcal{K}_s U^{n+1}, U^{n+1} \rangle = \|U^{n+1}\|_{\mathcal{K}_s}^2 \geq 0$ gives

$$\Big\langle A \, D_{\tau,\Delta}^{\alpha} U^{n+1}, \, U^{n+1} \Big\rangle \; + \; \|U^{n+1}\|_{\mathcal{K}_s}^2 \; \leq \; \langle \mathcal{N}(U^{n+1}), \, U^{n+1} \rangle, \tag{5.3}$$

where $D^{\alpha}_{\tau,\Delta}$ denotes the discrete Caputo operator ($\Delta\tau^{-\alpha}\sum_{k=0}^{n+1} g_k(\cdot)^{n+1-k}$). A standard coercivity inequality for the L1/GL operator yields

$$\left\langle A\, D^{\alpha}_{\tau,\Delta} U^{n+1},\, U^{n+1}\right\rangle \;\geq\; \frac{\|U^{n+1}\|_A^2 - \|U^{n}\|_A^2}{2\,\Delta\tau^{\alpha}}. \tag{5.4}$$

Assume that the nonlinear mapping $\mathcal{N}$ is locally Lipschitz in the A–norm on the numerical trajectory with constant L, and is treated implicitly. Then

$$\left\langle \mathcal{N}(U^{n+1}),\, U^{n+1}\right\rangle \;\leq\; L\,\|U^{n+1}\|_A^2. \tag{5.5}$$

Combining (5.3)–(5.5) we obtain

$$\frac{\|U^{n+1}\|_A^2 - \|U^{n}\|_A^2}{2\,\Delta\tau^{\alpha}} \;+\; \|U^{n+1}\|_{\mathcal{K}_s}^2 \;\leq\; L\,\|U^{n+1}\|_A^2. \tag{5.6}$$

Thus the fully discrete nonlinear scheme is *stable* provided

$$L\,\Delta\tau^{\alpha} \;\leq\; \tfrac{1}{2}, \tag{5.7}$$

in which case $\|U^n\|_A$ is nonincreasing and the discrete energy is dissipative. Next, we will discuss the computational results of the method.

6. Computational sesults and applications

In this section, we present the computational results to validate the theoretical findings. The numerical algorithm developed in Section 3 will be validated through the examination of test problems involving the migration and interaction of solitons. We utilize the L_2 and L_∞ error norms to quantify the disparity between the numerical and analytical solutions, thereby demonstrating the predictive accuracy of the scheme regarding the position and amplitude of the solution as the simulation progresses. The L_2 and L_∞ norms of the solution are defined as follows:

$$\begin{aligned} L_2 &= \|\nu^{exact} - \nu^n\|_2 = [h\sum_{i=1}^{N} |\nu_i^{exact} - \nu_i^n|^2]^{\frac{1}{2}}, \\ L_\infty &= \|\nu^{exact} - \nu^n\|_\infty = max_i|\nu_i^{exact} - \nu_i^n|. \end{aligned} \tag{6.1}$$

Also for $\varphi(\psi,\tau)$, the L_2 and L_∞ norms of the solution are defined as follows:

$$\begin{aligned} L_2 &= \|\varphi^{exact} - \varphi^n\|_2 = [h\sum_{i=1}^{N} |\varphi_i^{exact} - \varphi_i^n|^2]^{\frac{1}{2}}, \\ L_\infty &= \|\varphi^{exact} - \varphi^n\|_\infty = max_i|\varphi_i^{exact} - \varphi_i^n|. \end{aligned} \tag{6.2}$$

Example 6.1. First, we give the case of interaction of a single solitary wave. The initial conditions for this example is as follows

$$\nu(\psi,0) = \frac{1}{8}\lambda^2\left(1 - 4\mathrm{sech}^2\left(\frac{\lambda\psi}{2}\right)\right), \tag{6.3}$$

$$\varphi(\psi,0) = \lambda\mathrm{sech}\left(\frac{\lambda\psi}{2}\right). \tag{6.4}$$

$$\begin{aligned} &\nu(-10,\tau) = \nu(10,\tau) = 0, && \nu_\psi(-10,\tau) = \nu_\psi(10,\tau) = 0, \\ &\varphi(-10,\tau) = \varphi(10,\tau) = 0, && \varphi_\psi(-10,\tau) = \varphi_\psi(10,\tau) = 0. \end{aligned} \tag{6.5}$$

and the exact solution is

$$\nu(\psi,\tau) = \frac{1}{8}\lambda^2\left(1 - 4sech^2\left(\frac{\lambda}{2}\left(\psi + \frac{1}{2}\lambda^2\tau\right)\right)\right), \tag{6.6}$$

$$\varphi(\psi,\tau)=\lambda sech\left(\frac{\lambda}{2}\left(\psi+\frac{1}{2}\lambda^2\tau\right)\right). \tag{6.7}$$

TABLE 1. Error norms for $\nu(\psi,\tau)$ and $\varphi(\psi,\tau)$ at $\Delta\psi=0.02$,$\Delta\tau=0.001$ $\alpha=0.75$ and $\lambda=0.75$.

	$\nu(\psi,\tau)$		$\varphi(\psi,\tau)$	
τ	L_2	L_∞	L_2	L_∞
0.1	5.1197e-04	2.2420e-09	8.6545e-05	4.6024e-10
0.2	5.1235e-04	2.2475e-09	8.6622e-05	3.1777e-09
0.3	5.1273e-04	2.2529e-09	8.6699e-05	6.8161e-09
0.4	5.1311e-04	2.2582e-09	8.6776e-05	8.6124e-09
0.5	5.1350e-04	2.2635e-09	8.6853e-05	8.5388e-09
0.6	5.1388e-04	2.2687e-09	8.6930e-05	8.4648e-09
0.7	5.1426e-04	2.2738e-09	8.7008e-05	8.3905e-09
0.8	5.1464e-04	2.2789e-09	8.7085e-05	8.3159e-09
CPU time = 3.71 Sec				

Table 1 presents the error norms L_2 and L_∞ for the numerical solutions of $\nu(\psi,\tau)$ and $\varphi(\psi,\tau)$ at $\Delta\psi=0.02$, $\Delta\tau=0.001$, and $\alpha=0.75$.

TABLE 2. Error norms for $\nu(\psi,\tau)$ and $\varphi(\psi,\tau)$ at $\Delta\psi=0.02$,$\Delta\tau=0.001$ $\alpha=0.5$ and $\lambda=0.1$.

	$\nu(\psi,\tau)$		$\varphi(\psi,\tau)$	
τ	L_2	L_∞	L_2	L_∞
0.1	3.9898e-04	3.5242e-11	2.1622e-05	7.9708e-10
0.2	3.9899e-04	3.6184e-11	2.1627e-05	5.6975e-10
0.3	3.9901e-04	3.7127e-11	2.1631e-05	3.4241e-10
0.4	3.9902e-04	3.8069e-11	2.1636e-05	1.1506e-10
0.5	3.9903e-04	3.9012e-11	2.1641e-05	1.1230e-10
0.6	3.9905e-04	3.9954e-11	2.1646e-05	3.3966e-10
0.7	3.9906e-04	4.0896e-11	2.1651e-05	5.6704e-10
0.8	3.9907e-04	4.1838e-11	2.1655e-05	7.9442e-10
CPU time =0.77 Sec				

Table 2 presents the error norms L_2 and L_∞ for $\nu(\psi,\tau)$ and $\varphi(\psi,\tau)$ at $\Delta\psi=0.02$, $\Delta\tau=0.001$, and $\alpha=0.5$.

Table 3 shows the error norms L_2 and L_∞ for $\nu(\psi,\tau)$ and $\varphi(\psi,\tau)$ at $\Delta\psi=0.02$, $\Delta\tau=0.001$, and $\alpha=1$.

Table 4 provides the absolute errors for $\nu(\psi,\tau)$ and $\varphi(\psi,\tau)$ at $\Delta\psi=0.02$, $\Delta\tau=0.001$, and $\tau=0.3$ for different values of α. The errors decrease as α decreases, with the smallest errors observed for $\alpha=0.05$. This highlights the method's ability to handle fractional-order systems with high precision, particularly for smaller values of α.

Table 5 compares the numerical solutions of $\nu(\psi,\tau)$ obtained using the the Adomian Decomposition Transform Method (ADTM) [8] and PG-FEM methods for different values of α.

Table 6 compares the numerical solutions of $\varphi(\psi,\tau)$ obtained using ADTM [8] and PG-FEM methods for different values of α.

Figure 1 illustrates the numerical solutions of $\nu(\psi,\tau)$ and $\varphi(\psi,\tau)$ at $\tau=0.3$. The profiles exhibit smooth wave propagation, characteristic of the time-fractional Jaulent-Miodek system.

Figure 2 depicts the numerical solutions of $\nu(\psi,\tau)$ and $\varphi(\psi,\tau)$ at $\tau=1.20$. The results show controlled wave dispersion and minimal amplitude attenuation, consistent with the fractional-order dynamics of the system. The

TABLE 3. Error norms for $\nu(\psi,\tau)$ and $\varphi(\psi,\tau)$ at $\Delta\psi = 0.02$,$\Delta\tau = 0.001$ $\alpha = 1$ and $\lambda = 1$.

	$\nu(\psi,\tau)$		$\varphi(\psi,\tau)$	
τ	L_2	L_∞	L_2	L_∞
0.1	1.8536e-02	2.9390e-09	2.2104e-03	1.7497e-07
0.2	1.8536e-02	4.2440e-09	2.2604e-03	1.2214e-07
0.3	1.8535e-02	3.5744e-09	2.3118e-03	6.3687e-08
0.4	1.8534e-02	2.6295e-09	2.3647e-03	8.3585e-10
0.5	1.8533e-02	1.5500e-09	2.4190e-03	4.7004e-08
0.6	1.8532e-02	3.2423e-10	2.4748e-03	1.5008e-07
0.7	1.8531e-02	1.0600e-09	2.5322e-03	2.3588e-07
0.8	1.8530e-02	2.6156e-09	2.5911e-03	3.2991e-07
CPU time = 3.54 Sec				

TABLE 4. Absolute error and CPU time for $\nu(\psi,\tau)$ and $\varphi(\psi,\tau)$ at $\Delta\psi = 0.02$,$\Delta\tau = 0.001$ and $\tau = 0.3$.

	$\alpha = 1$		$\alpha = 0.5$		$\alpha = 0.05$	
ψ	$\nu(\psi,\tau)$	$\varphi(\psi,\tau)$	$\nu(\psi,\tau)$	$\varphi(\psi,\tau)$	$\nu(\psi,\tau)$	$\varphi(\psi,\tau)$
0	3.0574e-05	1.0702e-04	2.3579e-05	1.8043e-05	8.4589e-07	1.5114e-07
0.1	2.3527e-04	1.0790e-04	3.1337e-05	1.8960e-05	7.9886e-07	1.6232e-07
0.2	3.5806e-05	1.6219e-04	1.6849e-05	3.2573e-05	7.5631e-07	2.9840e-07
0.3	2.7140e-04	1.6287e-04	3.2365e-05	3.3572e-05	7.1342e-07	3.1089e-07
0.4	9.0267e-05	2.1061e-04	1.0574e-05	4.5733e-05	6.7631e-07	4.3313e-07
0.5	2.9714e-04	2.0983e-04	3.3502e-05	4.6452e-05	6.3703e-07	4.4317e-07
0.6	7.9014e-04	1.8714e-04	1.7721e-04	4.5553e-05	4.5651e-06	4.5120e-07
0.7	6.8098e-04	3.3328e-04	1.4497e-04	7.9655e-05	5.4169e-06	7.8460e-07
0.8	8.5061e-04	1.6127e-04	1.9436e-04	3.9130e-05	5.1089e-06	3.8720e-07
0.9	3.1400e-04	2.7557e-04	3.5733e-05	6.5511e-05	5.0765e-07	6.4228e-07
	CPU time =6.35 Sec		CPU time =6.15 Sec		CPU time =6.27 Sec	

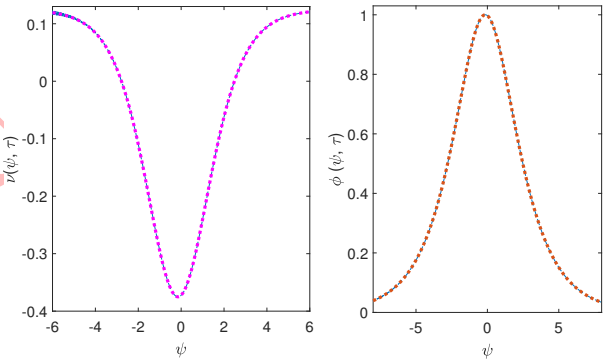

FIGURE 1. Numerical Solution of $\nu(\psi,\tau)$ and $\varphi(\psi,\tau)$ at $t = 0.3seconds$.

TABLE 5. The different fractional-order of α at $\nu(\psi,\tau)$ of Problem 1 [8].

ψ	*Method*	(τ)	$\alpha = 0.6$	$\alpha = 0.75$	$\alpha = 0.9$
0.2	$ADTM$	0.2	1.1486e-04	6.0217e-05	2.0349e-05
	$PG-FEM$		2.3338e-05	2.3655e-06	3.1999e-06
	$ADTM$	0.4	1.4900e-04	8.3844e-05	3.3041e-05
	$PG-FEM$		4.7609e-05	2.3657e-06	3.2064e-06
	$ADTM$	0.6	1.6158e-04	9.5489e-05	3.9611e-05
	$PG-FEM$		6.9063e-05	2.3658e-06	3.2129e-06
	$ADTM$	0.8	1.5881e-04	1.0046e-04	3.8667e-05
	$PG-FEM$		8.7461e-05	2.3660e-06	3.2193e-06
	$ADTM$	1.0	1.4305e-04	9.3646e-05	3.8577e-05
	$PG-FEM$		1.0267e-04	2.3662e-06	3.2258e-06
0.4	$ADTM$	0.2	2.0021e-04	1.0769e-04	3.7140e-05
	$PG-FEM$		8.0677e-05	2.1212e-06	2.9774e-06
	$ADTM$	0.4	2.4800e-04	1.4292e-04	5.1429e-05
	$PG-FEM$		9.9071e-05	2.1214e-06	2.9834e-06
	$ADTM$	0.6	2.4390e-04	1.4833e-04	5.6984e-05
	$PG-FEM$		1.1427e-04	2.1215e-06	2.9894e-06
	$ADTM$	0.8	2.2309e-04	1.4238e-04	5.7231e-05
	$PG-FEM$		1.2624e-04	2.1217e-06	2.9954e-06
	$ADTM$	1.0	1.8377e-04	1.2523e-04	5.2764e-05
	$PG-FEM$		1.3504e-04	2.1219e-06	3.0014e-06
	CPU time		6.14 Sec	6.13 Sec	4.88 Sec

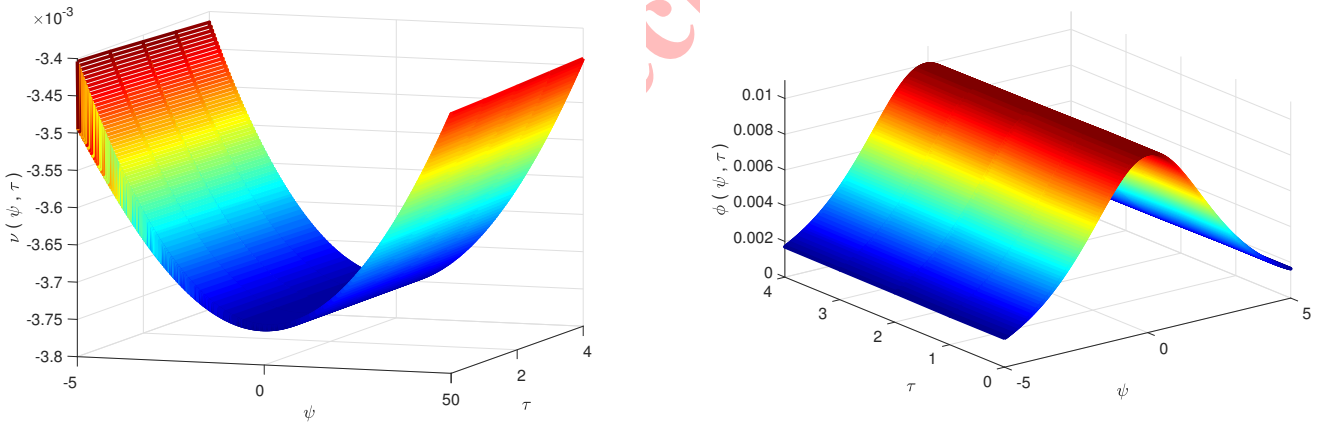

(A) Numerical Solution of $\nu(\psi,\tau)$. (B) Numerical Solution of $\varphi(\psi,\tau)$.

FIGURE 2. Numerical solutions of $\varphi(\psi,\tau)$ and $\nu(\psi,\tau)$ at $\tau = 1:20$ seconds.

preservation of wave coherence over extended time intervals underscores the method's robustness in handling long-term memory effects and nonlinearities. The solutions align with theoretical expectations, validating the numerical framework's reliability for simulating fractional-order wave phenomena.

TABLE 6. The different fractional-order of α at $\varphi(\psi,\tau)$ of Problem 1 [8].

ψ	Method	(τ)	$\alpha=0.6$	$\alpha=0.75$	$\alpha=0.9$	$\alpha=1$
0.2	ADTM	0.2	2.3041e-04	1.2072e-04	4.0782e-05	5.2168e-09
	PG-FEM		1.4826e-04	1.1954e-06	4.8174e-06	1.1925e-08
	ADTM	0.4	2.9956e-04	1.6838e-04	6.0359e-05	4.2984e-09
	PG-FEM		1.7569e-04	1.1984e-06	4.8648e-06	1.1925e-08
	ADTM	0.6	3.2581e-04	1.9297e-04	7.2298e-05	1.1229e-07
	PG-FEM		2.0130e-04	1.2014e-06	4.9121e-06	1.1926e-08
	ADTM	0.8	3.2153e-04	2.0013e-04	7.8209e-05	3.6381e-07
	PG-FEM		2.2487e-04	1.2043e-06	4.9593e-06	1.1927e-08
	ADTM	1.0	2.9142e-04	1.9179e-04	7.8540e-05	7.2998e-07
	PG-FEM		2.4624e-04	1.2073e-06	5.0064e-06	1.1928e-08
0.4	ADTM	0.2	4.0349e-04	2.1685e-04	7.4750e-05	1.0117e-08
	PG-FEM		1.9863e-04	1.7342e-06	6.9683e-06	1.7315e-08
	ADTM	0.4	4.8688e-04	2.8015e-04	1.0305e-04	8.2174e-09
	PG-FEM		2.2206e-04	1.7368e-06	7.0104e-06	1.7316e-08
	ADTM	0.6	4.9539e-04	2.9140e-04	1.1544e-04	2.8118e-07
	PG-FEM		2.4328e-04	1.7394e-06	7.0524e-06	1.7317e-08
	ADTM	0.8	4.5622e-04	2.9116e-04	1.1674e-04	5.7399e-07
	PG-FEM		2.6220e-04	1.7421e-06	7.0943e-06	1.7318e-08
	ADTM	1.0	3.8010e-04	2.5792e-04	1.0888e-04	1.3386e-06
	PG-FEM		2.7876e-04	1.7447e-06	7.1360e-06	1.7319e-08
1.0	ADTM	0.2	8.8541e-04	5.1163e-04	1.6963e-04	2.2521e-08
	PG-FEM		3.9764e-04	2.8625e-06	1.1465e-05	2.8612e-08
	ADTM	0.4	1.0049e-03	6.0421e-04	2.2306e-04	1.7910e-08
	PG-FEM		3.0689e-04	2.8638e-06	1.1485e-05	2.8612e-08
	ADTM	0.6	9.8125e-04	6.1570e-04	2.2650e-04	6.1461e-07
	PG-FEM		3.1398e-04	2.8650e-06	1.1505e-05	2.8613e-08
	ADTM	0.8	8.1123e-04	5.3908e-04	1.9708e-04	1.4601e-06
	PG-FEM		3.1904e-04	2.8663e-06	1.1525e-05	2.5767e-08
	ADTM	1.0	6.1485e-04	4.3470e-04	1.9056e-04	2.8662e-06
	PG-FEM		3.2221e-04	2.8675e-06	1.1544e-05	2.8613e-08

Example 6.2. Second, we give the case of interaction of a single solitary wave. The initial condition for the second problem s as follows

$$\nu(\psi,0) = s - \tfrac{1}{2}b_0 k\,\mathrm{sech}(k\psi) - \tfrac{3}{4}c_2\,\mathrm{sech}^2(k\psi),$$
$$\varphi(\psi,0) = b_0 + k\,\mathrm{sech}(k\psi),$$

and the boundary conditions as

$$\nu(-10,\tau) = \nu(10,\tau) = 0, \qquad \nu_\psi(-10,\tau) = \nu_\psi(10,\tau) = 0,$$
$$\varphi(-10,\tau) = \varphi(10,\tau) = 0, \qquad \varphi_\psi(-10,\tau) = \varphi_\psi(10,\tau) = 0. \tag{6.8}$$

The exact solution to the JM equation is of the form [35]

$$\nu(\psi,\tau) = s - \tfrac{b_0}{2}k\,\mathrm{sech}\left(k(R\tau+\psi)\right) - \tfrac{3c_2}{4}\,\mathrm{sech}^2\left(k(R\tau+\psi)\right),$$
$$\varphi(\psi,\tau) = b_0 + k\,\mathrm{sech}\left(k(R\tau+\psi)\right),$$

where

$$k = \sqrt{c_2}, \quad R = \frac{1}{2}\left(b_0^2 + c_2^2\right), \quad s = \frac{1}{4}\left(c_2 - b_0^2\right).$$

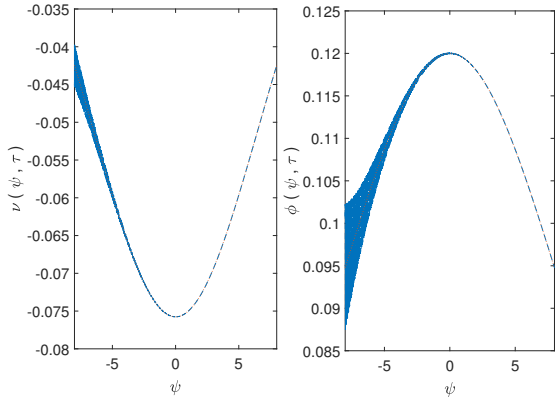

FIGURE 3. Numerical Solution of $\nu(\psi,\tau)$ and $\varphi(\psi,\tau)$ at $t = 1.5$ seconds and $\alpha = 0.75$.

The initial condition as shown

$$\begin{aligned} \nu(-10,\tau) = \nu(10,\tau) = 0, \qquad & \nu_\psi(-10,\tau) = \nu_\psi(10,\tau) = 0, \\ \varphi(-10,\tau) = \varphi(10,\tau) = 0, \qquad & \varphi_\psi(-10,\tau) = \varphi_\psi(10,\tau) = 0. \end{aligned} \tag{6.9}$$

TABLE 7. Error norm L_∞ for $\varphi(\psi,\tau)$ at $\Delta\psi = 0.02$, $\Delta\tau = 0.001$.

ψ	$\alpha = 1$ [35]	$\alpha = 1$	$\alpha = 0.05$	$\alpha = 0.5$
0.1	1.6105e-10	9.0758e-10	2.3630e-09	7.5645e-09
0.2	6.2775e-10	9.0870e-10	2.3624e-09	7.5643e-09
0.3	1.3488e-09	9.0982e-10	2.3618e-09	7.5641e-09
0.4	2.2318e-09	9.1094e-10	2.3611e-09	7.5638e-09
0.5	3.1376e-09	9.1206e-10	2.3605e-09	7.5636e-09
0.6	3.8782e-09	9.1094e-10	2.3598e-09	7.5634e-09
0.7	4.2181e-09	9.1431e-10	2.3592e-09	7.5631e-09
0.8	3.8832e-09	9.1543e-10	2.3585e-09	7.5629e-09
0.9	2.5762e-09	9.1655e-10	2.3579e-09	7.5627e-09
CPU time		1.43 Sec	2.09 Sec	2.07 Sec

Table 7 presents absolute maximum error (L_∞ norms) for the numerical solution of $\varphi(\psi,\tau)$ with discretization parameters $\Delta\psi = 0.02$ and $\Delta\tau = 0.001$. The results are compared with the B-spline solution [35] at $\alpha = 1$, demonstrating excellent agreement with the published work. Additionally, the table extends the analysis to fractional orders $\alpha = 0.05$ and $\alpha = 0.5$, revealing how error characteristics evolve with varying fractional parameters. The comparison shows that while all cases maintain high numerical precision, the error distribution exhibits distinct patterns across different α values, with the fractional cases displaying systematically larger errors compared to the integer-order case ($\alpha = 1$).

Table 8 presents the absolute errors for both $\nu(\psi,\tau)$ and $\varphi(\psi,\tau)$ at different values of the fractional order α ($\alpha = 1$ and $\alpha = 0.05$).

In figure 3The solutions exhibit characteristic subdiffusive behavior ($\alpha = 0.75$), with smooth spatial decay and memory-driven temporal evolution. Coupling between ν and φ is evident through phase alignment, while attenuated wavefronts reflect fractional damping.

Figure 4 demonstrates the transition from fractional ($\alpha = 0.75$) to classical ($\alpha = 1$) dynamics. The $\alpha = 0.75$ solutions exhibit characteristic subdiffusive behavior: smoothed spatial gradients and delayed temporal evolution due

TABLE 8. Absolute error for different fractional orders α at $\nu(\psi,\tau)$ and $\varphi(\psi,\tau)$ of Example 6.2.

ψ	τ	$\alpha=1$		$\alpha=0.05$	
		ν	φ	ν	φ
0.2	1	2.6865e-05	7.4850e-05	5.1597e-05	2.8131e-05
	5	2.6871e-05	7.4856e-05	5.1596e-05	2.8132e-05
	10	2.6879e-05	7.4863e-05	5.1596e-05	2.8133e-05
	15	2.6886e-05	7.4870e-05	5.1595e-05	2.8134e-05
	20	2.6894e-05	7.4877e-05	5.1594e-05	2.8135e-05
0.4	1	2.4451e-05	6.7182e-05	5.3364e-05	2.5145e-05
	5	2.4457e-05	6.7187e-05	5.3364e-05	2.5146e-05
	10	2.4464e-05	6.7193e-05	5.3363e-05	2.5147e-05
	15	2.4471e-05	6.7200e-05	5.3362e-05	2.5148e-05
	20	2.4478e-05	6.7206e-05	5.3362e-05	2.5149e-05
0.6	1	2.2331e-05	6.0354e-05	5.4939e-05	2.2483e-05
	5	2.2336e-05	6.0359e-05	5.4938e-05	2.2483e-05
	10	2.2343e-05	6.0365e-05	5.4938e-05	2.2483e-05
	15	2.2350e-05	6.0371e-05	5.4937e-05	2.2484e-05
	20	2.2356e-05	6.0377e-05	5.4937e-05	2.2484e-05
0.8	1	2.0472e-05	5.4278e-05	5.6341e-05	2.0102e-05
	15	2.0489e-05	5.4293e-05	5.6340e-05	2.0103e-05
	20	2.0495e-05	5.4298e-05	5.6339e-05	2.0104e-05
		CPU time= 1.43 Sec		CPU time= 2.09 Sec	

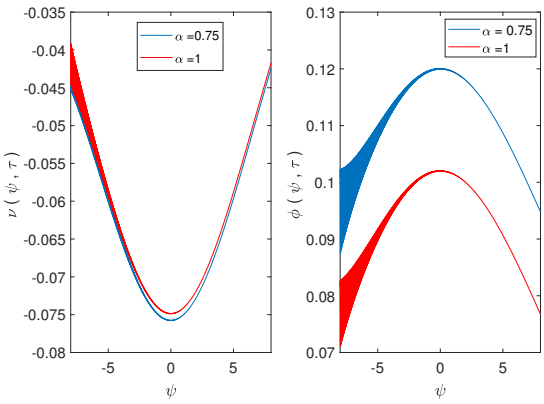

FIGURE 4. Numerical Solution of $\nu(\psi,\tau)$ and $\varphi(\psi,\tau)$ when $\alpha=0.75$ and $\alpha=1$.

to memory effects. In contrast, the $\alpha=1$ case shows sharper wavefronts and faster equilibration, consistent with standard diffusion/wave propagation. The persistent amplitude difference between ν and φ at $\alpha=0.75$ highlights stronger system memory coupling, while their convergence at $\alpha=1$ reflects Markovian behavior. This comparison validates the fractional model's capability to capture intermediate transport regimes between diffusion and wave propagation.

7. Conclusion

In this study, we developed and analyzed a Petrov–Galerkin finite element method (PG-FEM) based on quintic B-splines for solving the time-fractional Jaulent–Miodek (JM) coupled system with Caputo derivatives. Stability was established through Von Neumann analysis, and the method was shown to capture nonlinear wave phenomena with high accuracy, as verified by error norms and benchmark comparisons. The results confirm that fractional-order models yield deeper insights than classical integer-order formulations by effectively representing memory effects, anomalous transport, and dispersion characteristics. Numerical experiments further demonstrated the capability of the proposed scheme to resolve compactons, soliton interactions, and long-term wave propagation without spurious oscillations. Beyond accuracy, the framework offers practical advantages: quintic B-spline discretization improves precision, the Thomas algorithm enhances computational efficiency, and the method accommodates a wide range of fractional orders, including very small values of α. These features establish PG-FEM as a robust approach for studying nonlinear fractional PDEs relevant to viscoelasticity, porous media flow, nonlinear optics, and biological wave processes. Future directions include incorporating adaptive mesh refinement, hybrid spectral–finite element strategies, and validation through experimental comparisons to strengthen the physical applicability of the fractional JM system and further bridge the gap between mathematical modeling and real-world nonlinear wave phenomena. Future work will extend this study through adaptive mesh refinement, hybrid spectral–finite element strategies, and comparisons with experimental data to validate the physical relevance of the fractional JM system. In addition, a detailed error analysis will be conducted to rigorously validate the numerical results obtained with the proposed technique.

Funding

Not available.

Availability of data and materials

Not applicable.

Declarations

The authors declare that they have no competing interests.

Competing interests

All the authors declare no conflict of interest

Authors' contributions

The author has read and confirmed the final manuscript and participated equally in the manuscript.

Acknowldegmnt

The authors would like to thank the anonymous reviewers and editor for providing helpful comments and suggestions, which further improved the quality of the manuscript.

References

[1] A. Adiga, D. Dubhashi, B. Lewis, M. Marathe, S. Venkatramanan, and A. Vullikanti, *Mathematical Models for COVID-19 Pandemic: A Comparative Analysis*, J. Indian Inst. Sci., *100*(4) (2020), 793–807.

[2] I. Ahmad, H. Ahmad, P. Thounthong, Y. M. Chu, and C. Cesarano, *Solution of multi-term time-fractional PDE models arising in mathematical biology and physics by local meshless method*, Symmetry, *12*(7) (2020), 1195.

[3] S. Ahmad and A. T. Tiamiyu, *Numerical simulation of time-dependent non-Newtonian compressible fluid flow in porous media: Finite element method and time integration approach*, Int. Commun. Heat Mass Transf., *159* (2024), 107934.

[4] G. Ai, J. Yin, and L. Cui, *Learning Gravity Fields of Small Bodies: Self-adaptive Physics-informed Neural Networks*, Astron. J., *168*(6) (2024), 242.

[5] H. M. Ali, K. S. Nisar, W. R. Alharbi, and M. Zakarya, *Efficient approximate analytical technique to solve nonlinear coupled Jaulent-Miodek system within a time-fractional order*, AIMS Math., *9*(3) (2024), 5671–5685.

[6] A. A. Alikhanov, M. S. Asl, C. Huang, and A. Khibiev, *A second-order difference scheme for the nonlinear time-fractional diffusion-wave equation with generalized memory kernel in the presence of time delay*, J. Comput. Appl. Math., *438* (2024), 115515.

[7] Y. Alkhezi and A. Shafee, *Analytical Techniques for Studying Fractional-Order Jaulent–Miodek System Within Algebraic Context*, Fractal Fract., *9*(1) (2025), 50.

[8] S. Alshammari, M. M. Al-Sawalha, and R. Shah, *Approximate Analytical Methods for a Fractional-Order Nonlinear System of Jaulent–Miodek Equation with Energy-Dependent Schr"odinger Potential*, Fractal Fract., *7*(2) (2023), 140.

[9] M. Al-Smadi, O. A. Arqub, and D. Zeidan, *Fuzzy fractional differential equations under the Mittag-Leffler kernel differential operator of the ABC approach: Theorems and applications*, Chaos Solitons Fractals, *146* (2021), 110891.

[10] A. A. Alzahrani, *Numerical Analysis of Nonlinear Fractional System of Jaulent–Miodek Equation*, Symmetry, *15*(7) (2023), 1350.

[11] S. U. Arifeen, S. Haq, I. Ali, and S. F. Aldosary, *Galerkin approximation for multi-term time-fractional differential equations*, Ain Shams Eng. J., *15*(7) (2024), 102806.

[12] O. Avit and H. Anac, *The Novel Conformable Methods To Solve Conformable Time-Fractional Coupled Jaulent-Miodek System*, Eskisehir Tech. Univ. J. Sci. Tech. A, *25*(1) (2024), 123–140.

[13] N. Bhangale, K. B. Kachhia, and J. F. Gomez-Aguilar, *Fractional viscoelastic models with Caputo generalized fractional derivative*, Math. Methods Appl. Sci., *46*(7) (2023), 7835–7846.

[14] Q. Cao, S. Goswami, and G. E. Karniadakis, *Laplace neural operator for solving differential equations*, Nat. Mach. Intell., *6*(6) (2024), 631–640.

[15] M. Cinar, I. Onder, A. Secer, M. Bayram, T. A. Sulaiman, and A. Yusuf, *Solving the fractional Jaulent–Miodek system via a modified Laplace decomposition method*, Waves Random Complex Media, (2022), 1–14.

[16] A. K. Gombert and J. Nielsen, *Mathematical modelling of metabolism*, Curr. Opin. Biotechnol., *11*(2) (2000), 180–186.

[17] M. A. Hammad, A. W. Alrowaily, R. Shah, S. M. Ismaeel, and S. A. El-Tantawy, *Analytical analysis of fractional nonlinear Jaulent-Miodek system with energy-dependent Schr"odinger potential*, Front. Phys., *11* (2023), 1148306.

[18] K. Hattaf, *On the Stability and Numerical Scheme of Fractional Differential Equations with Application to Biology*, Computation, *10*(6) (2022), 97.

[19] S. B. G. Karakoc and S. K. Bhowmik, *Galerkin finite element solution for Benjamin–Bona–Mahony–Burgers equation with cubic B-splines*, Comput. Math. Appl., *77*(7) (2019), 1917–1932.

[20] G. E. Karniadakis, I. G. Kevrekidis, L. Lu, P. Perdikaris, S. Wang, and L. Yang, *Physics-informed machine learning*, Nature Rev. Phys., *3*(6) (2021), 422–440.

[21] B. Li, T. Zhang, and C. Zhang, *Investigation of financial bubble mathematical model under fractal-fractional Caputo derivative*, Fractals, *31*(5) (2023), 2350050.

[22] T. Liu and S. Shateyi, *Efficient Fourth-Order Weights in Kernel-Type Methods without Increasing the Stencil Size with an Application in a Time-Dependent Fractional PDE Problem*, Mathematics, *12*(7) (2024), 1121.

[23] F. Mostajeran and S. M. Hosseini, *Solving Multi-Term Time-Fractional Diffusion Equations Using a High-Order Fractional Finite Difference Scheme Accompanied by Neural Network Techniques*, Numer. Methods Partial Differ. Equ., *41*(1) (2025), 1–20.

[24] M. Ozisik, A. Secer, M. Bayram, M. Cinar, N. Ozdemir, H. Esen, and I. Onder, *Investigation of optical soliton solutions of higher-order nonlinear Schr"odinger equation having Kudryashov nonlinear refractive index*, Optik, *274* (2023), 170548.

[25] N. K. Pal, P. Chatterjee, and A. Saha, *Solitons, multi-solitons and multi-periodic solutions of the generalized Lax equation by Darboux transformation and its quasiperiodic motions*, Int. J. Mod. Phys. B, *38*(30) (2024), 1–20.

[26] M. Ramadan and H. Samy, *New approach for solving of Extended KdV Equation*, Alfarama J. Basic Appl. Sci., (2022), 1–15.
[27] M. Ramadan, H. Samy, I. Hanafy, and W. Adel, *Petrov–Galerkin finite element method for solving the time-fractional Rosenau–Hyman equation*, J. Umm Al-Qura Univ. Appl. Sci., (2025), Article in press.
[28] H. Samy, W. Adel, I. Hanafy, and M. Ramadan, *A Petrov–Galerkin approach for the numerical analysis of soliton and multi-soliton solutions of the Kudryashov–Sinelshchikov equation*, Iran. J. Numer. Anal. Optim., *14*(4) (2024), 1309–1335.
[29] S. M. Sayed, A. S. Mohamed, E. M. Abo El-Dahab, and Y. H. Youssri, *Alleviated Shifted Gegenbauer Spectral Method for Ordinary and Fractional Differential Equations*, Contemp. Math., *5*(2) (2024), 2123–2149.
[30] S. M. Sayed, A. S. Mohamed, E. M. Abo-Eldahab, and Y. H. Youssri, *Spectral framework using modified shifted Chebyshev polynomials of the third-kind for numerical solutions of one- and two-dimensional hyperbolic telegraph equations*, Bound. Value Probl., *2025*(1) (2025), 7.
[31] M. Şenol, O. Iyiola, H. Kasmaei, and L. Akinyemi, *Efficient analytical techniques for solving time-fractional nonlinear coupled Jaulent–Miodek system with energy-dependent Schr"odinger potential*, Adv. Differ. Equ., *2019*(1) (2019), 1–21.
[32] G. Shen, J. Manafian, S. Zia, D. Huy, and T. Le, *The New Solitary Solutions to the Time-Fractional Coupled Jaulent-Miodek Equation*, Discrete Dyn. Nat. Soc., *2021*(1) (2021), 2429334.
[33] J. Weickert, B. Romeny, and M. Viergever, *Efficient and reliable schemes for nonlinear diffusion filtering*, IEEE Trans. Image Process., *7*(3) (1998), 398–410.
[34] Y. Youssri, S. Sayed, A. Mohamed, E. Aboeldahab, and W. Abd-Elhameed, *Modified Lucas polynomials for the numerical treatment of second-order boundary value problems*, Comput. Methods Differ. Equ., *11*(1) (2023), 12–31.
[35] W. Zahra, W. Ouf, and M. El-Azab, *Numerical simulation for the solution of nonlinear Jaulent–Miodek coupled equations using quartic B-spline*, Acta Univ. Apulensis, *46* (2016), 35–52.